Thermal discrete element method for transient heat conduction in granular packing under compressive forces

Kiani-Oshtorjani Mehran, Jalali Payman

DOI: 10.1016/j.ijheatmasstransfer.2019.118753

Thermal discrete element method for transient heat conduction in granular packing under compressive forces

Mehran Kiani-Oshtorjani[a,b,*], Payman Jalali[a,b]

[a] *Laboratory of Thermodynamics, School of Energy Systems, Lappeenranta University of Technology, Lappeenranta, Finland*
[b] *SIM-Platform, Lappeenranta University of Technology, Lappeenranta, Finland*

Abstract

A thermal discrete element method is introduced in granular packs. This method is applicable to 3D packing in either static or dynamic states coupled with the ordinary discrete element method code. This method resolves the local heat fluxes and temperature of particles relying on particles conductivity and the deformation of particles at various contact points. Using this method, the time evolution of temperature is studied within packed beds under various compressive forces. Our results match very well with the analytical solution as if the value of the effective conductivity is properly adjusted, which is found to be related to the pressure exponentially. We have also shown that the compression of the granular packing exponentially increases the thermal characteristic time of the bed.

Keywords: Energy Equation, Discrete Element Method, Granular Packed Bed, Temperature Distribution, Heat Conduction

1. Introduction

Granular materials are found extensively in nature as well as industrial processes from energy, food processing, manufacturing and chemical technologies. In the technologies related to the energy production in packed beds or fluidized beds, the thermal performance of plants is directly linked to the behavior of the particulate medium as the main carrier of thermal energy controlled by the known mechanisms of conduction, convection and radiation.

*Corresponding author
Email addresses: mehran.kiani@lut.fi (Mehran Kiani-Oshtorjani), payman.jalali@lut.fi (Payman Jalali)

Nomenclature

α_T	thermal diffusivity	$[\frac{m^2}{s}]$
$\bar{m}$	reduced mass	$[kg]$
$\bar{Q}_{jP}$	flux on contact j of particle P	$[W]$
$\boldsymbol{\alpha_i}$	angular acceleration	$[\frac{1}{s^2}]$
$\boldsymbol{a_i}$	linear acceleration	$[\frac{m}{s^2}]$
$\boldsymbol{e_n}$	unit vector in n direction	
$\boldsymbol{e_t}$	unit vector in t direction	
$\boldsymbol{g}$	gravity acceleraton	$[\frac{m}{s^2}]$
$\boldsymbol{v_r}$	relative velocity	$[\frac{m}{s}]$
$\boldsymbol{v_s}$	relative slip velocity	$[\frac{m}{s}]$
δ_m	mean overlap	$[m]$
δ_n	normal overlap	$[m]$
δ_t	tangential displacement	$[m]$
η_n	damping coefficient in n direction	$[\frac{N.s}{m}]$
η_t	damping coefficient in t direction	$[\frac{N.s}{m}]$
κ_P	heat conductivity of particle P	$[\frac{W}{m.K}]$
κ_{eff}	effective thermal conductivity of bed	$[\frac{W}{m.K}]$
μ	friction coefficient	
ϕ	angle	$[rad]$
ρ	particle density	$[kg/m^3]$
σ	Poisson's ratio	
θ	angle	$[rad]$
c_P	specific heat capacity	$[\frac{J}{kg.K}]$
d	particle diameter	$[m]$
E	Young's modulus	$[Pa]$
G	shear modulus	$[Pa]$
I_i	moment of inertia	$[kg.m^2]$
K_n	spring stiffness in n direction	$[\frac{N}{m}]$
K_t	spring stiffness in t direction	$[\frac{N}{m}]$
L	length of bed	$[m]$
m_i	particle mass	$[kg]$
P_f	Legendre polynomials	
P_{fg}	associated Legendre polynomials	
q	heat flux	$[\frac{W}{m^2}]$
R_c	packed bed radius	$[m]$
R_P	particle radius	$[m]$
S_i	surface area of contact i	$[m^2]$
T	temperature	$[K]$
T_P^0	temperature at the center of particle P	$[K]$
T_P^i	temperature at contact i of particle P	$[K]$

Granular materials have been theoretically studied using both the Eulerian and Lagrangian approaches. The Eulerian approach treats the granular medium as a continuum. The interactions of existing phases (gas-solid or solid-solid) within a control volume are represented by proper correlations that specify an average volumetric estimation of forces. There have been a number of studies adopting Eulerian methods, e.g. Jalali et al. [1] for modelling the hydrodynamics of circulating fluidized beds using multiphase Eulerian method, as well as Kiani-Oshtorjani and Jalali [2] for modelling the hydrodynamic and thermal characteristics of packed beds using a novel lattice Boltzmann method. Other alternatives to the Eulerian approach to simulate heat transfer between granular particles are finite element method (FEM) [3, 4] and lattice element method (LEM) [5, 6].

Unlike the continuum description of particulate systems in Eulerian approach, the Lagrangian approach sees individual particles and tracks them every time step. The well-known Lagrangian approach applied extensively in simulations of granular materials is the discrete element method (DEM) that is used to build static packs, Suikkanen et al. [7] , or to analyze the dynamics of particle mixtures, Jalali and Hyppanen [8].

The thermal analysis of packed beds is performed by solving the energy equation for particles configuration subject to proper boundary conditions. Siu and Lee [9] assigned each particle a uniform temperature given at its center. In this approach known as the thermal network, a number of heat pipes are assumed between particles through which heat fluxes transport to other particles. There is a thermal resistance for each connection (contact). As Feng et al. [10] mentioned, this model mostly relies on an ad-hoc manner, not on a theoretical base.

Feng et al. [10, 11] suggested a 2D model based on the boundary element method (BEM), which first resolved the steady state and then the transient condition inspired by the thermal network method. They presented an analytical solution to the energy equation at steady state for an individual particle subject to the Neumann boundary condition. Then they assigned an accurate temperature to the particle using a boundary integral method. The heat fluxes were obtained from the contacts of particle with neighbouring particles. Their work was limited to 2D space as they admitted they could not find any integral solution for 3D geometries.

He et al. [12] proposed a numerical manifold method (NMM) to model transient heat conduction in granular materials. In this model, some elementary geometries like circles, squares, or their combinations are defined to inscribe the particles known as mathematical covers. Then using the intersections between particles and mathematical covers, some manifold elements are extracted.

The manifold elements are defined without any overlap between the elements. It is argued in that paper that unlike FEM as a continuum approach, and thermal discrete element method (TDEM) as a discrete approach, the NMM can describe both continuum and discrete views to the problem. In other words, this model resembles the FEM, where, the temperature step changes at contact interfaces are included in the model, too.

In the studies of heat conduction in granular materials, the effective thermal conductivity (ETC) of the packed bed is a characteristic quantity. There are a number of studies to obtain this parameter theoretically [13, 14, 15], computationally [3], or experimentally [16, 17, 18].

Liang [19, 14] utilized the thermal resistance presented by Feng et. al. [10] to derive a theoretical formula for the ETC. They applied the formula to a 2D packed bed under a uniform strain. This formula was obtained based on a parallel-column model in which the granular bed was constructed by particle columns. Then the ETC of each column was obtained from the corresponding thermal resistance. The ETC of entire bed was calculated from the ETC of each column.

Kovalev and Gusarov [20] presented theoretical relation for ETC based on statistical mechanics. They also simulated the thermal behaviour of different packed beds consisted of different particle shapes. They employed the thermal resistance proposed by Feng et al. [10] for 2D problems to calculate the heat flux between particles.

The aim of the present paper is to introduce a thermal DEM approach for resolving transient heat conduction in 3D granular packing. The results of this study present the propagation of heat in different packed beds under various compressive pressures.

2. Thermal discrete element method

This section contains the derivation of TDEM. It starts with finding a steady-state solution to the heat conduction equation. By adding the transient term to the balance equation, the transient heat transfer equation will be obtained.

2.1. Solution of heat conduction equation

Our starting point for TDEM is to find an analytical solution to the Laplace equation (heat conduction) in spherical coordinate system. This equation is written with the Neumann boundary

condition on the boundary $\partial\Omega$ in the spherical domain Ω as:

$$\begin{aligned} \kappa_P \nabla^2 T = 0 \qquad & in \quad \Omega \\ \kappa_P \frac{\partial T}{\partial r} = q(\theta,\phi) \qquad & on \quad \partial\Omega \end{aligned} \tag{1}$$

where, θ and ϕ are the spherical angular coordinates as depicted in Fig. (1a), q is heat flux, and κ stands for the thermal conductivity of particles. The solution of the Laplace equation in spherical coordinate system can be obtained based on separation of variables as:

$$T(r,\theta,\phi) = \sum_{f=0}^{\infty}\sum_{g=0}^{f}\big(A_f r^f + \frac{B_f}{r^{f+1}}\big)P_{fg}(cos\phi)\big(C_g sin(g\theta) + D_g cos(g\theta)\big) + T_P^0 \tag{2}$$

where, f and g are the summation indices, T_P^0 is the temperature at the center of particle P, and the functions P_{fg} are Legendre polynomials.

Considering the azimuthally symmetric case where T does not depend on θ, i.e. $g = 0$, and the boundary condition at the center of sphere leading to $B_f = 0$, Eq. (2) is simplified as:

$$T(r,\phi) = \sum_{f=0}^{\infty} A_f r^f P_f(cos(\phi)) + T_P^0 \tag{3}$$

where, the coefficients A_f should be determined based on the boundary condition on $\partial\Omega$ which finally yields:

$$A_f = \frac{2f+1}{2f R_P^{f-1}\kappa}\int_0^{\pi} q(\psi)P_f(cos(\psi))sin(\psi)d\psi \tag{4}$$

By substituting Eq. (4) into (3), we obtain:

$$T(r,\phi) = \frac{R_P}{\kappa_P}\int_0^{\pi} q(\psi)sin(\psi)\sum_{m=1}^{\infty}\frac{2m+1}{2m}\big(\frac{r}{R_P}\big)^m P_m(cos\psi)P_m(cos\phi) \quad d\psi + T_P^0 \tag{5}$$

The mean temperature T_P^i on the i-th contact, and the flux $\bar{Q}_{jP}$ on any contact j can be calculated as:

$$T_P^i = \frac{1}{S_i}\int_{S_i} T_P^i(\theta,\phi)dS = \frac{2\pi R_P^2}{S_i}\int_0^{\phi_i} T_P^i(\phi)sin(\phi)d\phi \tag{6}$$

$$\bar{Q}_{jP} = 2\pi R_P^2 \int_{\phi_{j1}}^{\phi_{j2}} q_{jP}(\phi)sin\phi d\phi \tag{7}$$

where, S_i is the surface area of contact i, and ϕ_{j1} and ϕ_{j2} are the angles characterizing the influential region of contact j in the direction ϕ. In Eq. (6), $T_P^i(\phi)$ is the temperature distribution over the contact surface i of particle P obtained from Eq. (5) after substituting $r = R_P$ and breaking the integral to the summation over influential regions of all the contacts (covering the entire surface of particle), which yields:

$$T_P^i(\phi) = \frac{R_P}{\kappa_P} \sum_{j=1}^{k} \int_{\phi_{j1}}^{\phi_{j2}} q_{jP}(\psi) sin(\psi) \sum_{m=1}^{\infty} \frac{2m+1}{2m} P_m(cos\psi) P_m(cos\phi) \quad d\theta d\psi + T_P^0 \tag{8}$$

As a result, the mean temperature on contact i can be estimated by combining Eqs. (8) and (6):

$$T_P^i = \frac{2\pi R_P^2}{S_i} \frac{R_P}{\kappa_P} \sum_{j=1}^{k} \int_0^{\phi_i} \int_{\phi_{j1}}^{\phi_{j2}} q_{jP}(\psi) sin(\psi) sin(\phi) \sum_{m=1}^{\infty} \frac{2m+1}{2m} P_m(cos\psi) P_m(cos(\phi)) \quad d\psi d\phi + T_P^0 \tag{9}$$

By assuming a constant flux for each contact $q_{jP}(\psi) = \bar{q}_{jP}$, Eq. (7) will be:

$$\bar{Q}_{jP} = S_j \bar{q}_{jP} = 2\pi R_P^2 \bar{q}_{jP} \big(cos(\phi_{j1}) - cos(\phi_{j2})\big) \tag{10}$$

and using the identity of $cos(2x) = 1 - 2sin^2(x)$ we have:

$$\bar{Q}_{jP} = 4\pi R_P^2 \bar{q}_{jP} \big(sin^2(\frac{\phi_{j2}}{2}) - sin^2(\frac{\phi_{j1}}{2})\big) = 4\pi R_P^2 \bar{q}_{jP} \big(sin(\frac{\phi_{j2}}{2}) - sin(\frac{\phi_{j1}}{2})\big)\big(sin(\frac{\phi_{j2}}{2}) + sin(\frac{\phi_{j1}}{2})\big) \tag{11}$$

then, by considering $\phi_{j2} = \phi_{j1} + \Delta\phi_j$ and using the identity of $sin(\frac{\phi_{j2}}{2}) = sin(\frac{\phi_{j1}}{2} + \frac{\Delta\phi_j}{2}) = sin(\frac{\phi_{j1}}{2})cos(\frac{\Delta\phi_j}{2}) + sin(\frac{\Delta\phi_j}{2})cos(\frac{\phi_{j1}}{2}) \cong sin(\frac{\phi_{j1}}{2}) + \frac{\Delta\phi_j}{2} cos(\frac{\phi_{j1}}{2})$, Eq. (11) simplifies to:

$$\bar{Q}_{jP} = 2\pi R_P^2 \bar{q}_{jP} \Delta\phi_j cos(\frac{\phi_{j1}}{2}) \big(sin(\frac{\phi_{j2}}{2}) + sin(\frac{\phi_{j1}}{2})\big) \tag{12}$$

Substituting $\bar{q}_{jP}$ from Eq. (12) into Eq. (9) yields:

$$T_P^i = \sum_{j=1}^{k} \big[\frac{R_P \bar{Q}_{jP}}{\kappa_P S_i \Delta\phi_j cos(\frac{\phi_{j1}}{2}) \big(sin(\frac{\phi_{j1}}{2}) + sin(\frac{\phi_{j2}}{2})\big)} \times \int_0^{\phi_i} \int_{\phi_{j1}}^{\phi_{j2}} sin(\psi) sin(\phi) \sum_{m=1}^{\infty} \frac{2m+1}{2m} P_m(cos\psi) P_m(cos\phi) \quad d\psi d\phi \big] + T_P^0 \tag{13}$$

Christoffel-Darboux identity [21] guarantees that $\sum_{m=1}^{\infty}(2m+1)P_m(cos\psi)P_m(cos\phi)$ converges to -1, hence, $\sum_{m=1}^{\infty}\frac{2m+1}{2m}P_m(cos\psi)P_m(cos\phi)$ will converge to a negative constant λ, which is computationally obtained as -0.6846. Consequently, Eq. (13) can be simplified as:

$$T_P^i = \sum_{j=1}^{k} \frac{R_P \bar{Q}_{jP} \lambda}{\kappa_P S_i \Delta\phi_j cos(\frac{\phi_{j1}}{2})\big(sin(\frac{\phi_{j1}}{2}) + sin(\frac{\phi_{j2}}{2})\big)} \int_{\phi_{j1}}^{\phi_{j2}} sin(\psi) \int_0^{\phi_i} sin(\phi) d\phi d\psi + T_P^0 \tag{14}$$

Eventually, by using $S_i = \pi R_P^2 sin^2(\phi_i) \approxeq \pi R_P^2 \phi_i^2$ and $\int_0^{\phi_i} sin(\phi)d\phi = 1 - cos(\phi_i) = 2sin^2(\frac{\phi_i}{2}) \approxeq \frac{\phi_i^2}{2}$, we can reduce Eq. (14) to:

$$T_P^i = \sum_{j=1}^{k} \frac{\bar{Q}_{jP} \lambda}{2\kappa_P \pi R_P \Delta\phi_j cos(\frac{\phi_{j1}}{2})\big(sin(\frac{\phi_{j1}}{2}) + sin(\frac{\phi_{j2}}{2})\big)} \int_{\phi_{j1}}^{\phi_{j2}} sin(\psi) d\psi + T_P^0 \tag{15}$$

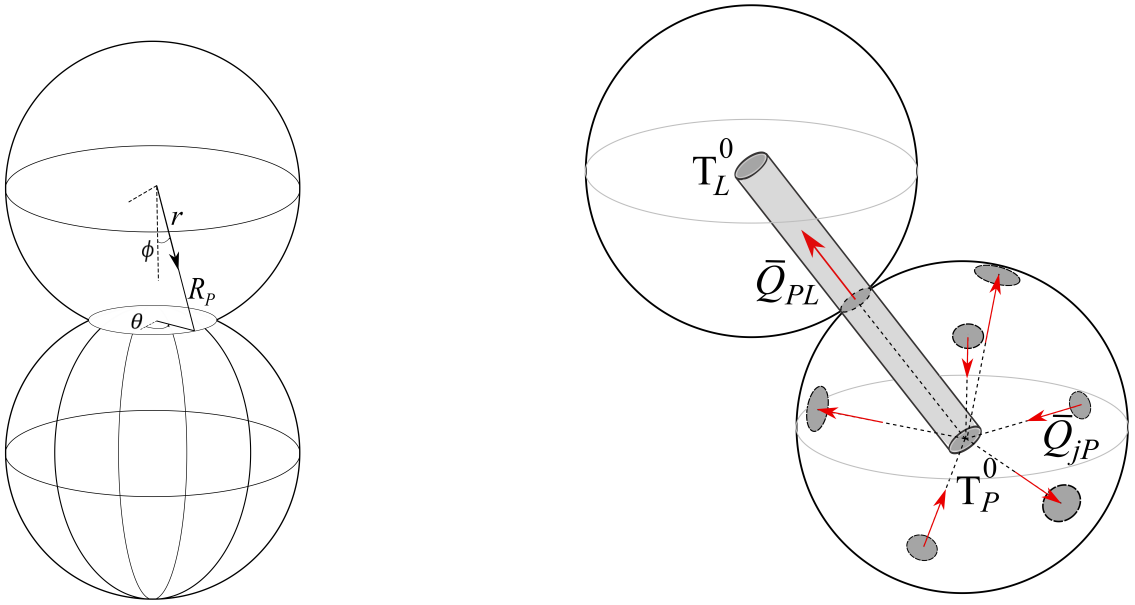

(a) (b)

Figure 1: Schematic of (a) contacting particles in spherical coordinate system (b) the pipe model connecting contact areas to the center of particles.

2.2. Two particle pipe model

For a central particle making several contacts with its neighboring particles, we note that Eq. (15) determines the temperature of any contact area i based on all the contacts of the central

particle. The main idea behind the two-particle pipe thermal model is to take into account the accumulative effects from the contacting particles on the temperature of contact i. In other words, the heat is exchanged between contact areas and the center of particle P, where all the fluxes contribute in building up any of heat fluxes exchanged between the contact area i and the central particle P as shown in Fig. (1b). In the pipe model, a pipe is attached to each contact through which a heat flux is transferred between the neighbouring particle and the central particle. In addition, the share of any contact j on T_P^i depends on the contact position represented by $\frac{\int_{\phi_{j1}}^{\phi_{j2}} sin(\psi)d\psi}{cos(\frac{\phi_{j1}}{2})\big(sin(\frac{\phi_{j1}}{2})+sin(\frac{\phi_{j2}}{2})\big)}$ in Eq. (15) assuming that $\bar{Q}_{jP}$ and $\Delta\phi_j$ are in the same order for all contacts. Thus, effective values of these two quantities can be introduced for the contact i and taken out of the summation. This simplifies Eq. (15) to the following equation:

$$T_P^i = \frac{\bar{Q}_{LP}\lambda}{2\kappa_P \pi R_P \Delta\phi_i} \sum_{j=1}^{k} \frac{\int_{\phi_{j1}}^{\phi_{j2}} sin(\psi)d\psi}{cos(\frac{\phi_{j1}}{2})\big(sin(\frac{\phi_{j1}}{2}) + sin(\frac{\phi_{j2}}{2})\big)} + T_P^0 \tag{16}$$

in which the value of $\sum_{j=1}^{k} \frac{\int_{\phi_{j1}}^{\phi_{j2}} sin(\psi)d\psi}{cos(\frac{\phi_{j1}}{2})\big(sin(\frac{\phi_{j1}}{2})+sin(\frac{\phi_{j2}}{2})\big)}$ is computationally calculated to be π. Note that ϕ_{j1} and ϕ_{j2} correspond to the contact j.

Eventually, Eq.(16) reaches to a final form after substituting the summation by π, which results in :

$$T_P^i = \frac{\bar{Q}_{LP}\lambda}{2\kappa_P R_P \Delta\phi_i} + T_P^0 \tag{17}$$

As a result, one can consider a pipe with the heat flow $\bar{Q}_{LP}$ and thermal resistance of $Re_P = \frac{-\lambda}{2\kappa_P R_P \Delta\phi_i}$ in the particle P side connecting the centers of two particles. According to this definition of the thermal resistance Re_P, it is inversely proportional to the deformation angle characterized by $\Delta\phi_i$. Equivalently, the effective conductivity between particles increases proportional to the deformation angle.

Consider two particles P and L assuming $T_P^0 > T_L^0$ and write the conservation equation for thermal energy. The direction of energy flux is from particle P toward particle L across the contact areas i and m of particles P and L, respectively. Thus the temperature at the i-th contact of particle P, T_P^i, due to the heat flux from particle L can be determined from Eq. (17) as,

$$T_P^i = -Re_P \bar{Q}_{PL} + T_P^0 \tag{18}$$

On the other hand, the temperature at the m-th contact of particle L, T_L^m, due to the flux from

particle P is calculated as,

$$T_L^m = Re_L \bar{Q}_{PL} + T_L^0 \tag{19}$$

where $Re_P = \frac{-\lambda}{2\kappa_P R_P \Delta\phi_i}$ and $Re_L = \frac{-\lambda}{2\kappa_L R_L \Delta\phi_m}$. Obviously, we have $T_P^i = T_L^m$ and $\Delta\phi_i = \Delta\phi_m$. By subtracting Eq. (19) from Eq. (18), we reach to the following equation for heat flux:

$$k_{PL} \begin{bmatrix} 1 & -1 \\ -1 & 1 \end{bmatrix} \begin{bmatrix} T_P^0 \\ T_L^0 \end{bmatrix} = \begin{bmatrix} Q^{PL} \\ -Q^{PL} \end{bmatrix} \tag{20}$$

where $k_{PL} = 1/(Re_P + Re_L)$.

Balancing the steady and transient terms in the heat conservation equation will yield the transient energy equation. Therefore, the energy equation governing the transient heat conduction in any individual particle p can be presented by,

$$C_P \dot{T}_P^0(t) + \sum_{J=1}^{N} Q_{PJ} = 0 \tag{21}$$

where J stands for the neighbour particles having contact with particle P. In addition, using Eq. (20) we have $Q_{PJ} = k_{PJ}(T_J^0 - T_P^0)$, and $C_P = \frac{4}{3}\pi\rho R^3 c_P$. This equation can be solved by marching in time.

3. Discrete Element Method

In the discrete element method (DEM), the trajectory of any individual particle is calculated through successive time steps. Starting from an initial non-overlapping configuration of particles with certain initial velocity distribution, particle-particle and wall-particle overlaps are created in time. The overlaps create normal forces as well as history-dependent frictional forces and torques in all contact areas. As a result of having forces and torques at each time step, the translational and angular accelerations are known, which in turn, the velocity and position of particles are determined by proper integrations in time. It is worth mentioning that the contact forces are represented by a spring-dashpot model [22]. The Hertzian theory [13] relating the force and deformation of particles is employed to calculate the normal and tangential force components for a linear spring-dashpot model at contact points as [23, 8]:

$$\boldsymbol{F_n} = \big(- K_n \delta_n^{\frac{3}{2}} - \eta_n \boldsymbol{v_r}.\boldsymbol{e_n} \big) \boldsymbol{e_n} \tag{22}$$

$$\boldsymbol{F_t} = \big(- K_t \boldsymbol{\delta_t} - \eta_n \boldsymbol{v_s} \big) \tag{23}$$

Here, K_n and K_t stand for spring normal and tangential stiffnesses, η_n and η_t are for damping coefficients of dashpots in the normal $\boldsymbol{e_n}$ and tangential $\boldsymbol{e_t}$ directions, respectively. In addition, the direction of $\boldsymbol{F_n}$ always relies on the unit vector $\boldsymbol{e_n}$ which is along the centerline of two particles i and j. The normal overlapping δ_n vector is simply calculated from the position of the centers of contacting particles and tangential displacement δ_t is obtained from $\delta_t = F_t/K_t$. Moreover, the direction of frictional (tangential) force $\boldsymbol{F_t}$ is determined from the direction of relative slip velocity $\boldsymbol{v_s}$. The relative velocities of $\boldsymbol{v_s}$ and $\boldsymbol{v_r}$ are as follows:

$$\boldsymbol{v_r} = \boldsymbol{v_i} - \boldsymbol{v_j} \tag{24}$$

$$\boldsymbol{v_s} = \boldsymbol{v_r} - (\boldsymbol{v_r}.\boldsymbol{n})\boldsymbol{e_n} + 0.5(d_i \boldsymbol{\omega_i} + d_j \boldsymbol{\omega_j}) \times \boldsymbol{e_n} \tag{25}$$

where d and $\boldsymbol{\omega}$ are the diameter and angular velocity of a particle, respectively. It should be emphasized that Eq. (23) is only valid for sliding condition. In static condition, the tangential component of force should be calculated by $\boldsymbol{F_t} = -\mu |F_{Cnij}| \boldsymbol{e_t}$ in which μ is the friction coefficient.

It should be mentioned that the normal and tangential spring stiffnesses K_n, K_t are obtained using the Hertzian contact theory for contacting spheres as follows:

$$K_n = \frac{4\sqrt{R_i R_j}}{3\big(\frac{1-\sigma_i^2}{E_i} + \frac{1-\sigma_j^2}{E_j}\big)\sqrt{R_i + R_j}} \tag{26}$$

$$K_t = \frac{8\sqrt{R_i R_j}}{3\big(\frac{1-\sigma_i^2}{G_i} + \frac{1-\sigma_j^2}{G_j}\big)\sqrt{R_i + R_j}} \delta_n^{\frac{1}{2}} \tag{27}$$

Here, σ, E, and $G = E(1+\sigma)/2$ are Poisson's ratio, Young's modulus, and shear modulus, respectively. It is worth mentioning that the contact of particles and wall can be resolved using the same normal stiffness expression in which the radius of wall tends to infinity. On the other hand, the normal and tangential dashpot coefficients may be taken equal as:

$$\eta_n = \eta_t = \alpha (\bar{m} K_n)^{\frac{1}{2}} \delta_n^{\frac{1}{4}} \tag{28}$$

where $\bar{m} = (\frac{1}{m_i} + \frac{1}{m_j})^{-1}$ is the reduced mass. α is a function of restitution coefficient e as:

$$\alpha = \frac{-\sqrt{5}ln(e)}{\sqrt{\pi^2 + ln^2(e)}} \tag{29}$$

The net force and torque on a particle is the summation on all contacts as follows:

$$\boldsymbol{F_i} = \sum_j (\boldsymbol{F_{nij}} + \boldsymbol{F_{tij}}) \tag{30}$$

$$\boldsymbol{T_i} = \frac{1}{2} \sum_j (d_i \boldsymbol{e_n} \times \boldsymbol{F_{tij}}) \tag{31}$$

Consequently, the linear and angular accelerations can be calculated as:

$$\boldsymbol{a_i} = \frac{\boldsymbol{F_i}}{m_i} + \boldsymbol{g} \tag{32}$$

$$\boldsymbol{\alpha_i} = \frac{\boldsymbol{T_i}}{I_i} \tag{33}$$

where $\boldsymbol{g}$ is gravitational acceleration and I_i is the moment of inertia of particle i.

4. Results and Discussion

In this section, a comparison is performed between the current model and other models in literature including the FEM. Then the packed beds under investigation are described and in continuation, the code is validated by comparing the results of simulations with analytical solution. Finally, the impact of compressive pressure on thermal conductivity is presented in different packed beds under various compressive pressures.

4.1. Present model versus existing ones

Considering two colliding particles, Batchelor and O'Brien [24], Carslow [25] and Yovanovich [26] have independently presented the following analytical formula for thermal conductivity assuming the same physical properties for both particles as:

$$k_{BOB} = 2\kappa_P \left(\frac{3F_n(1-\sigma^2)R_P}{4E}\right)^{\frac{1}{3}} \tag{34}$$

where, F_n is the magnitude of normal contact force. In addition, Argento and Bouvard [27] have argued that Batchelor and O'Brien (BOB) formula is confined to small deformations. They tried to

modify the BOB relation by introducing a fitting parameter calculated based on FEM simulations. Their proposed formula is:

$$k_{AB} = \frac{\pi}{2\beta}\kappa_P\big(\frac{3F_n(1-\sigma^2)R_P}{4E}\big)^{\frac{1}{3}} \tag{35}$$

in which the fitting parameter β is reported as 0.899. Later, Ott [28, 29] used the same analogy by performing other FEM simulations and reported 0.952 as the value of parameter β. It is worth mentioning that according to Refs. [30, 31, 32], the basis of these models relies on uniform temperature distribution assumption inside particles which needs some modifications. They considered the conductivity of surrounding fluid as a reason to make the temperature distribution inside particles as non-uniform. Then they modified the thermal resistance by adding an additional term for a non-uniform temperature distribution. This additional term is only characterized by the surrounding fluid properties. Moreover, another source for non-uniform temperature distribution inside an individual particle is different contacts through which various heat fluxes coming in or going out of particle.

On the other hand, by using the definition of thermal resistance, we can derive a new thermal conductance formula as:

$$k_{New} = \frac{-2\kappa_P}{\lambda}\frac{1}{\frac{1}{R_P\Delta\phi_i}+\frac{1}{R_L\Delta\phi_m}} \tag{36}$$

By considering the same radius for particles, $R_P\Delta\phi_i = R_L\Delta\phi_m$. Then Eq. (36) will be reduced to:

$$k_{New} = \frac{-\kappa_P}{\lambda}R_P\Delta\phi_i \tag{37}$$

The value of $R_P\Delta\phi_i$ can be calculated using Euclid's formula which is: $[R_P\Delta\phi_i]^2 = (R_P^2 - (R_P - \frac{\delta_n}{2})^2) = R_P\delta_n$. The normal deformation δ_n will be obtained by assuming two particles at rest and using Eq. (22) as $\delta_n = (\frac{F_n}{K_n})^{\frac{2}{3}}$. As a result, we can conclude that:

$$R_P\Delta\phi_i = \sqrt{R_P}(\frac{F_n}{K_n})^{\frac{1}{3}} \tag{38}$$

On the other hand, Eq. (26) will be simplified to the following equation by considering the same physical properties for both contacting particles:

$$K_n = \frac{4E}{6(1-\sigma^2)}\sqrt{\frac{R_P}{2}} \tag{39}$$

By substituting Eq. (39) into (38) and Eq. (38) into (37), the thermal conductivity will be obtained as:

$$k_{New} = 2.066\kappa_P\big(\frac{3F_n(1-\sigma^2)R_P}{4E}\big)^{\frac{1}{3}} \tag{40}$$

The thermal conductivity obtained in Eq. (40) is similar to the BOB equation presented in Eq. (34). The thermal conductivity of a contacting pair of particles, with the physical properties tabulated in Table (1), are plotted versus the imposed load in Fig. (2b). As this figure illustrates, the new equation is pretty close to the BOB model (~ 3 percent difference). However, the difference with other equations could be due to the fact that the effects of all contacts are accumulated in the new model. As a result, a higher heat flux makes a higher thermal conductance.

By introducing $\zeta = \left(\frac{3F_n(1-\sigma^2)R_P}{4E}\right)^{\frac{1}{3}}$ and two dimensionless parameters of $\frac{R_P}{\zeta}$ and $\xi = \frac{\kappa_P R_P}{2\kappa_{PL}}$, the new model is compared with other models, including FEM simulations of [29], in Fig.(2b). This figure depicts the new model is fairly close to the BOB model as well as FEM simulations.

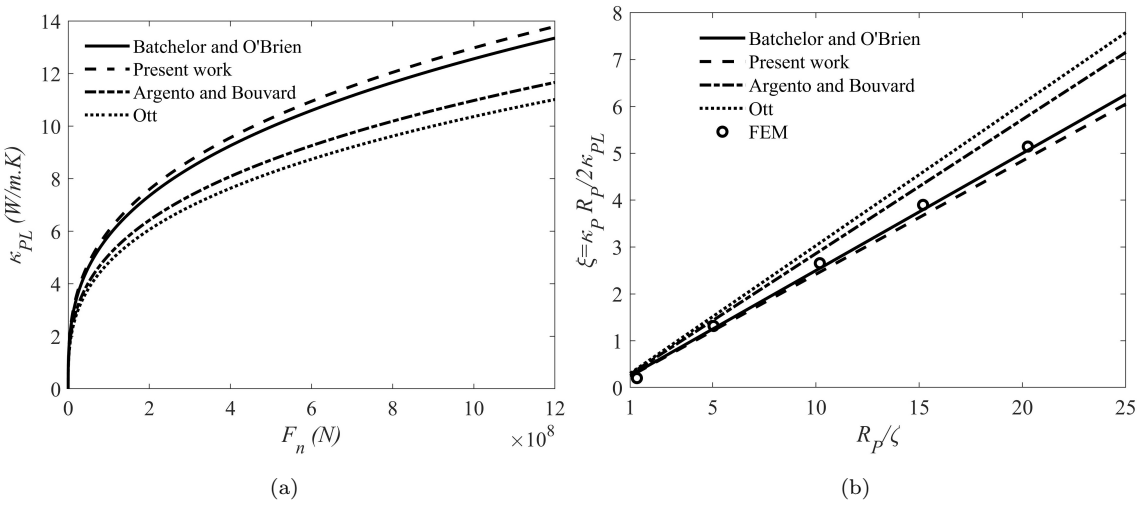

Figure 2: Comparison of various models for (a) thermal conductivity versus normal compressive force (b) dimensionless parameter ξ versus dimensionless parameter $\frac{R_P}{\zeta}$.

4.2. Case study

The studied case is a cylindrical packed bed built using the DEM code in which a non-overlapping dilute particle configuration settles down under gravitational force to create a dense packed bed. The radius of packed bed is $R_c = 30.5\ mm$ which contains 7500 particles with the physical properties of aluminium listed in Table (1). It is worth mentioning that the performance of the model should not be dependent of physical properties including the range of thermal conductivity.

To construct the packed bed, the position of non-overlapping particles are generated randomly

inside the cylindrical chamber. Then they fall down under gravity and eventually stack a dense pack. After completion of particles settlement, the system is compressed by moving the upper plate downward with the rate of 4 $\frac{mm}{s}$ for a certain time to deliver a desired compressive force. The granular packed bed is illustrated in Fig. (3). This figure demonstrates two packed beds under the compressive forces of 4770 N (left) and 1.184×10^5 N (right). The corresponding pressures are 16 bar and 405 bar, respectively. The particles configuration under the achieved compressive force is taken to perform the calculations of the conduction problem, which will be presented in Sec. 4.4. The height of the bed is decreased by 12.1 mm (3.025 d) and 2.9 mm (0.725 d) due to the compressive forces of 1.184×10^5 N and 4770 N, respectively. It can be directly observed from the two stacks that compression leads to highly ordered packing. The detailed analysis of packing structures with their connection to the compression and heat conduction will be studied in future works.

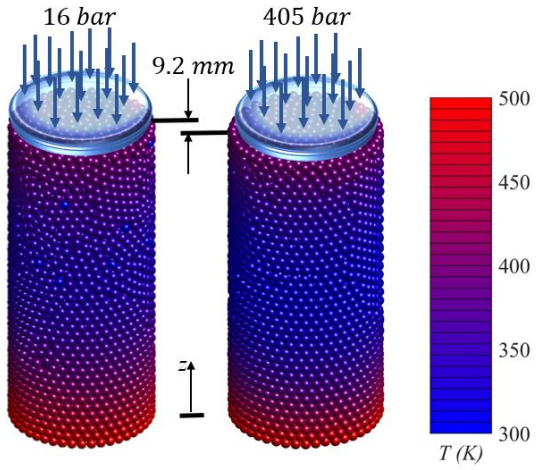

Figure 3: Packed beds used in simulations; (left) the compressive force of 4770 N (pressure of 16 bar) exerted on the bed and (right) the compressive force of 1.184×10^5 N (pressure of 405 bar). Colors of particles represent their temperatures at $t = 0.5$ s.

The force exerted on the upper plate during the compression is plotted versus time in Fig (4). In fact, this force is obtained while the upper plate moves downward with a uniform rate of 4 $\frac{mm}{s}$. Before looking into the dependence of the ETC on the compressive pressure, one may have an insight into the possible role of structural characteristics. For this purpose, we find the azimuthal angle of contacts, shown by ϕ_c, which is measured for each contact of the central particle in the coordinate

system attached to the particle as shown in Fig. (1a). Figure (5) demonstrates the probability distribution function (PDF) of ϕ_c in the two packs compressed with 16 and 405 bars. Interestingly, the fingerprint of high compression can be observed as a peak appearing at $\phi_c \approx \pi/3$ for the high pressure of 405 bar. Moreover, the PDF at high pressure relatively drops in $\pi/6 < \phi_c < \pi/3$. The decrease of contacts in this range of ϕ_c can reduce the vertical heat flux (the direction of imposed temperature gradient). This leads to the reduction of the effective conductivity in vertical direction. Note that the decay of PDF within $\pi/2 > \phi_c > 2\pi/5$ for high pressure is not as important as that within $\pi/6 < \phi_c < \pi/3$. This is because the role of horizontally oriented contacts is of less importance as they are perpendicular to the temperature gradient carrying insignificant heat fluxes.

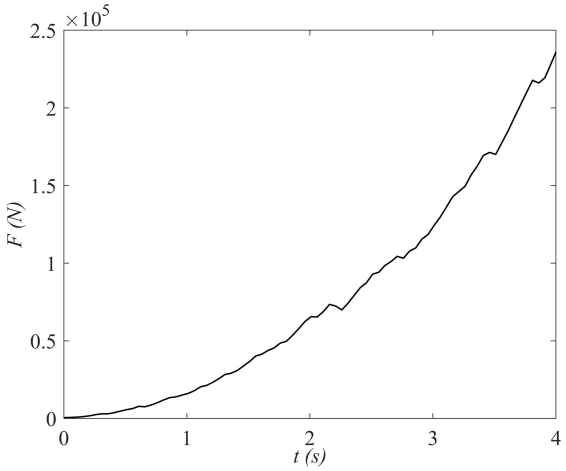

Figure 4: Variation of the force exerted on the upper plate versus time during compression.

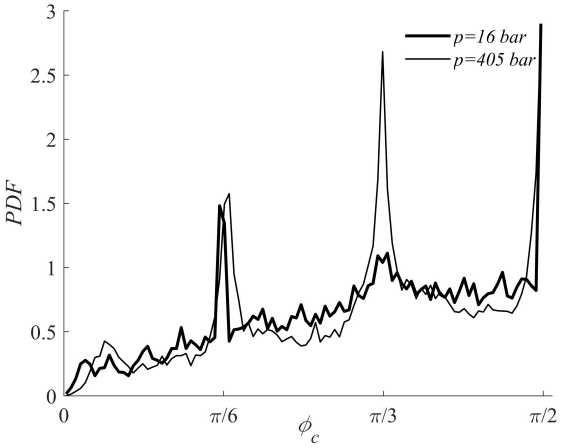

Figure 5: Probability distribution function (PDF) of azimuthal angular position of contacts measured in coordinates attached to central particles.

4.3. Comparison to analytical solution

The results of the TDEM code is performed are compared to the analytical predictions presented in Appendix A. Two distinguished thermal cases are considered, in both of which the temperature at the bottom of bed is kept at 500 K. In the first case, the top wall and initial temperatures of entire particles are set to 300 K and 400 K, respectively. In the second case, the top wall and initial temperatures of entire particles are set to 400 K and 300 K, respectively. The temperatures of the top and bottom walls are kept fixed in time for both cases.

Table 1: Simulation parameters.

particle density	ρ	$2500\frac{kg}{m^3}$
particle radius	R_P	$0.002m$
Radius of packed bed	R_c	$0.0305m$
Poissons ratio of particle	σ	0.2
restitution coefficient	e	0.865
modulus of longitudinal elasticity	E	$5 \times 10^{10} Pa$
friction coefficient	μ	0.3
gravity Acceleration	g	$9.81\frac{m}{s^2}$
thermal conductivity	κ	$205\frac{W}{m.K}$
specific heat	c_P	$900\frac{J}{kg.K}$

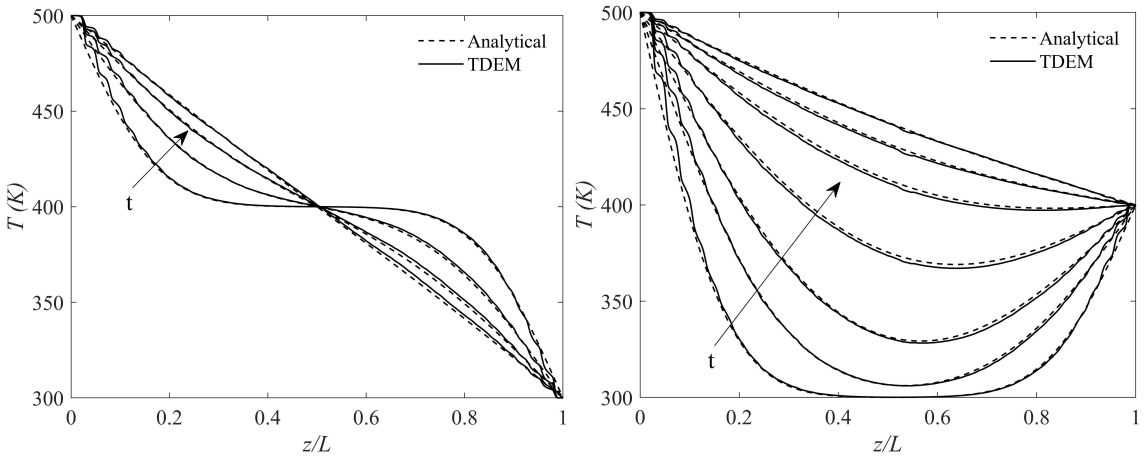

Figure 6: Temperature profile at different times for analytical (dash line) and TDEM (solid line) results for (a) first case and (b) second case. (a) Temperature of the bottom and top walls are 500 K and 300 K, respectively. Initial temperature of particles is 400 K. Different lines represent the times of $t = 0.2, 0.5, 1.0, 2.0$ s. (b) Temperature of the bottom and top walls are 500 K and 400 K, respectively. Initial temperature of particles is 300 K. Different lines for the times of $t = 0.2, 0.5, 1.0, 2.0, 3.5, 5.0, 7.0$ s. The arrows show the direction of time increase in both parts.

Figure (6a) depicts the temperature profile along the bed for the first case obtained from the

analytical solution and the TDEM. For TDEM, the mean temperature is calculated for any bin centered at a cross section of given heights. Mean temperature of a bin is calculated as the weighted average of particles temperatures within the bin weighted by the partial volume of particles lying in the bin. The results shown in Fig. (6a) indicate that the TDEM results matches closely to the analytical solution. Additionally, the results corresponding to the second case are demonstrated in Fig. (6b). These results also confirm that the TDEM data closely match to those of the analytical solution in various times.

It should be noted that in the analytical solution presented in Appendix A, the ETC of the bed is present in the formulas. The ETC can be assumed proportional to the particle conductivity as $\kappa_{eff} = \gamma\kappa_P$, in which κ_P is the particle thermal conductivity and γ is the coefficient of proportionality [33, 34, 35]. This coefficient γ can be obtained by matching the TDEM and analytical results in any packing under a certain compressive pressure, which is shown in Fig. (7). This figure indicates that γ depends on the compressive pressure exponentially, which means it drops sharply with pressure by an order of magnitude with little changes within a wide range of pressure increase.

4.4. Effect of compressive pressure on thermal conduction

In this section, the compressive pressure on the packed bed is varied and it is demonstrated how it affects on the thermal conduction features. First, the profiles of temperature are shown in Figs. (8a)-(8d) at different times for 4 different pressures ranging from 0.28 bar to 405 bar. The boundary values of temperature are 500 K and 400 K for the bottom and top walls, respectively. The initial temperature of bed particles is 300 K. As Fig. (8) illustrates, the compressive pressure delays the evolution of temperature profile to the steady one. The temperature profile already develops to the steady one at $t = 2$ s for the pressure of 0.28 bar, while it is still under development for the greater pressures. It is evident that as pressure rises, the delay in developing the temperature profile increases. The thermal response of the system becomes fairly similar for the compressive pressures of 155 bar and 405 bar.

In order to clarify the time evolution of temperature under various compressive pressures, the variation of temperature at the middle of the bed is demonstrated with time in Fig. (9) for the compressive pressures mentioned above. An immediate observation from this figure is that the local temperature reaches to the steady state value much earlier in the lowest pressure than those in the

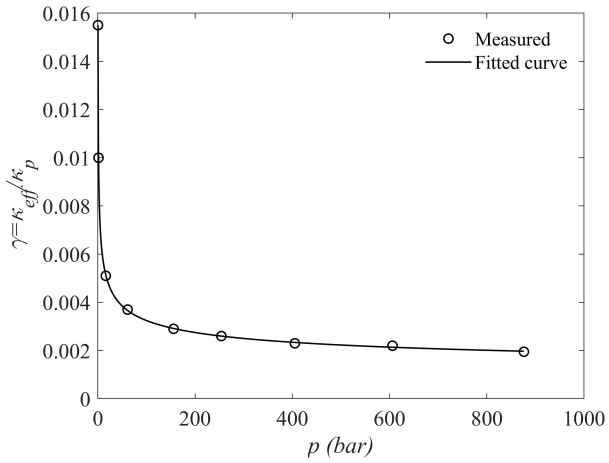

Figure 7: Variation of γ vs. compression pressure. The fitted function for γ is obtained as $\gamma = 0.01039p^{-0.2919} + 5.353 \times 10^{-4}$.

higher pressures. Therefore, one may define a conduction characteristic time as,

$$\tau = \frac{\int_0^\infty (T_{steady} - T)dt}{T_{steady} - T_{init}} \tag{41}$$

Here, T_{steady} is the steady state temperature, T_{init} is the initial temperature and $T(t)$ is the temperature of the section as a function of time. The variation of the characteristic time in the packs under different compressive pressures are shown versus the compressive pressure in Fig. (10). This figure reveals that the characteristic time increases with compressive pressure in a power of pressure as about 0.1, that is, it increases rapidly in lower pressures below 80 *bar* and it grows in a slower rate beyond this pressure.

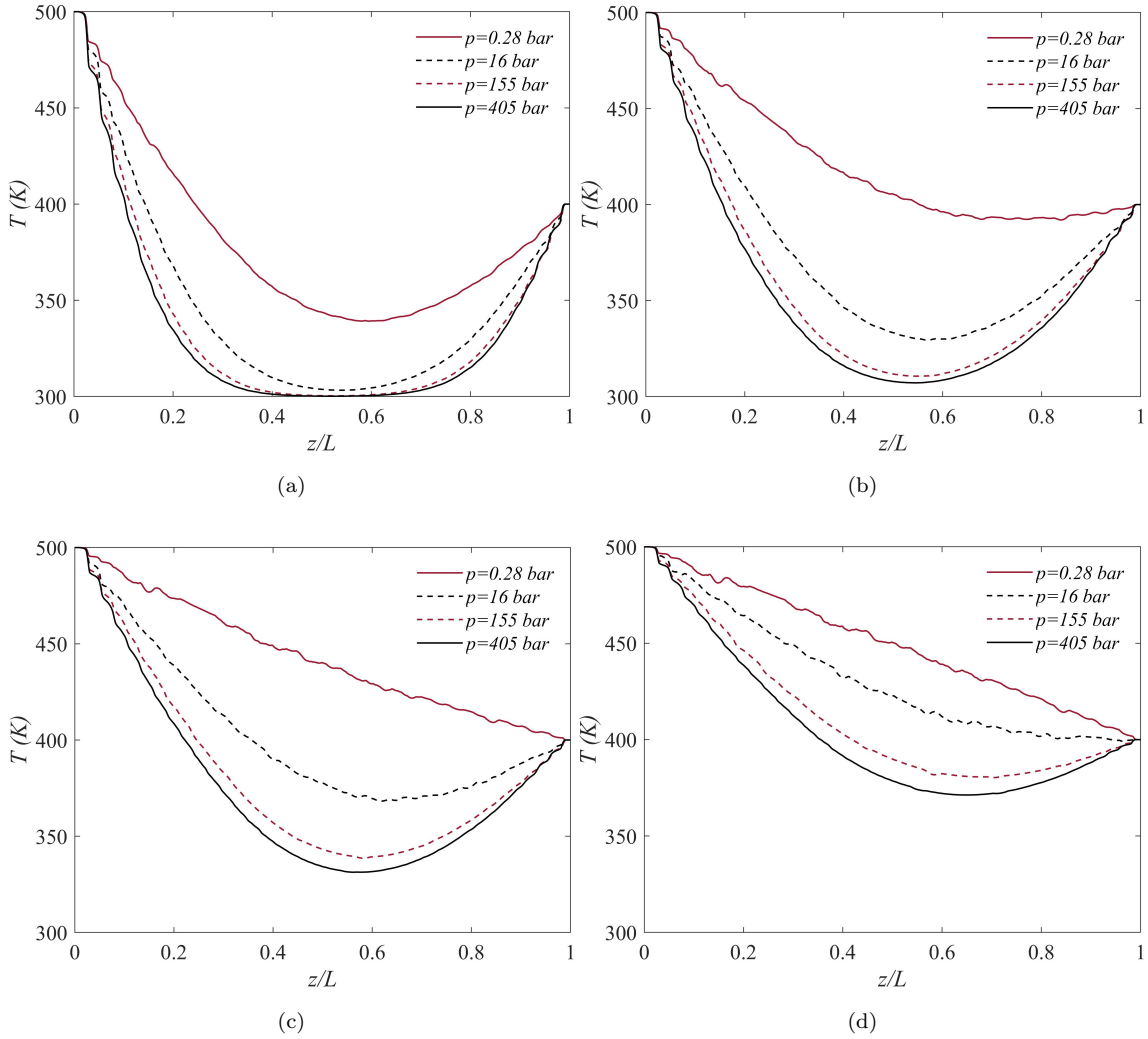

Figure 8: Temperature profiles in the packed beds under different compressive pressures at (a) 0.2 s (b) 0.5 s (c) 1 s (d) 2 s .

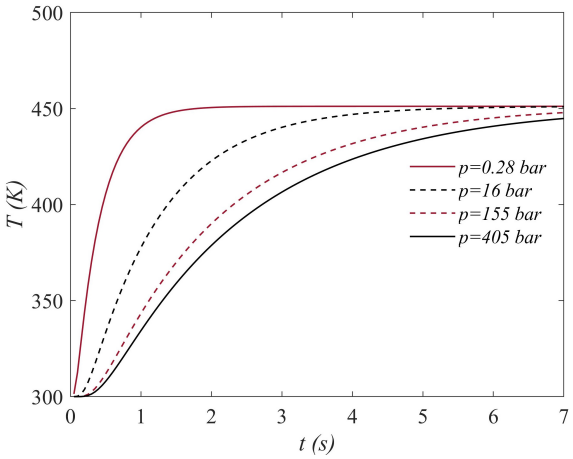

Figure 9: Time evolution of temperature at the middle of packed bed under different compressive pressures.

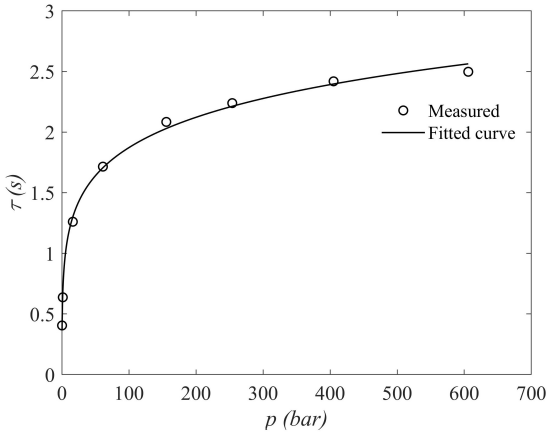

Figure 10: Variation of conduction characteristic time versus compressive pressure. The fitted line is $\tau = 1.945p^{0.1084} - 1.332$.

5. Conclusion

In this paper, a novel thermal discrete element method (TDEM) is introduced to resolve heat conduction in the packs of spherical particles, though it can be also extended to any arbitrary shape of particles. This model can be implemented in both static and dynamic packs with transient heat conduction. Simulations were performed on various dense packs generated using an in-house code of DEM. The dense packs were obtained by releasing non-overlapping particles to settle at the bottom of a cylindrical container due to the gravity. After the gravity driven settlement, the upper plate was pushed down with a small constant velocity to exert a desired compressive pressure on the bed. The compressed bed was then fed to the TDEM code to perform conduction simulations. First, the code was validated by the analytical solution in which the ratio of medium conductivity to the particle conductivity was obtained by matching up the TDEM solution with the analytical solution. Then the simulation code was utilized to determine how the compressive pressure affects the conduction by showing the evolution of temperature profiles in time under various pressures. Also, the conduction characteristic time was calculated based on the local variation of temperature under different compressive pressures. These results revealed that the effective conductivity of the packed bed is proportional to the particle thermal conductivity and the coefficient of proportionality depends on the compressive pressure exponentially. Moreover, it was shown that increasing

the compressive pressure slows down the heat conduction, which can be connected to the role of pressure in decreasing the effective conductivity. In this regard, it was demonstrated that the conduction characteristic time is described by a power function of the pressure. The decay of effective conductivity with pressure may be associated with the changes in contacts and the mean direction of the centerlines at contact points. This will be investigated in future studies in details.

Appendix A: Analytical solution of energy equation

Here, the energy equation of (A1) is analytically solved for granular packed beds. By averaging the solid volume fraction (SVF) over each cross section, the 3D problem is simplified to 1D problem with the equation as:

$$\frac{\partial T}{\partial t} = \alpha_T \frac{\partial^2 T}{\partial x^2} \qquad in \quad \Omega \tag{A1}$$

which is subject to the initial and boundary conditions of:

$$\begin{aligned} T(0,t) &= T_0 \\ T(L,t) &= T_L \\ T(x,0) &= T_{init} \end{aligned} \tag{A2}$$

Here, $\alpha_T = \frac{\kappa_{eff}}{\rho C_p}$ is the thermal diffusivity and κ_{eff} is the effective thermal conductivity of bed. Introducing $T(x,t) = v(x) + w(x,t)$, the problem can be simplified as:

$$\frac{\partial w}{\partial t} = \alpha_T \frac{\partial^2 w}{\partial x^2} \qquad in \quad \Omega \tag{A3}$$

with the initial and boundary conditions of:

$$\begin{aligned} w(0,t) &= T_0 - v(0) \\ w(L,t) &= T_L - v(L) \\ w(x,0) &= T_{init} - v(x) \end{aligned} \tag{A4}$$

As a result, $v(x)$ should be such that the boundary conditions are homogeneous, i.e., $v(x) = T_0 + \frac{x}{L}(T_L - T_0)$. Therefore, the final solution for $T(x,t)$ is obtained as:

$$T(x,t) = T_0 + \frac{x}{L}(T_L - T_0) + \sum_{m=1}^{\infty} C_m exp(-\frac{m^2\pi^2\alpha_T t}{L^2}) sin(\frac{m\pi x}{L}) \tag{A5}$$

where,

$$C_m = \frac{2}{m\pi} T_{in}\left[1-(-1)^m\right] + \frac{2}{m\pi}\left[(-1)^m T_L - T_0\right] \tag{A6}$$

Acknowledgment

Authors would like to acknowledge the financial support for this work by the SIM-Platform at LUT, and also the Academy of Finland under Grant No. 311138.

References

[1] P. Jalali, M. Nikku, J. Ritvanen, T. Hyppänen, Flow characteristics of circulating fluidized beds near terminal velocity: Eulerian model of a lab-scale apparatus, Powder technology 339 (2018) 569–584.

[2] M. Kiani-Oshtorjani, P. Jalali, Thermal and hydraulic properties of sphere packings using a novel lattice Boltzmann model, International Journal of Heat and Mass Transfer 130 (2019) 98–108.

[3] H. Zhang, Y. Zhao, F. Wang, D. Li, A 3D discrete element-finite difference coupling model for predicting the effective thermal conductivity of metal powder beds, International Journal of Heat and Mass Transfer 132 (2019) 1–10.

[4] J. Chen, H. Wang, L. Li, Determination of effective thermal conductivity of asphalt concrete with random aggregate microstructure, Journal of Materials in Civil Engineering 27 (12) (2015) 4015045.

[5] A. S. Sattari, Z. H. Rizvi, H. B. Motra, F. Wuttke, Meso-scale modeling of heat transport in a heterogeneous cemented geomaterial by lattice element method, Granular Matter 19 (4) (2017) 66.

[6] Z. H. Rizvi, D. Shrestha, A. S. Sattari, F. Wuttke, Numerical modelling of effective thermal conductivity for modified geomaterial using lattice element method, Heat and Mass Transfer 54 (2) (2018) 483–499.

[7] H. Suikkanen, J. Ritvanen, P. Jalali, R. Kyrki-Rajamäki, Discrete element modelling of pebble packing in pebble bed reactors, Nuclear Engineering and Design 273 (2014) 24–32.

[8] P. Jalali, T. Hyppänen, Momentum transport between two granular phases of spherical particles with large size ratio: two-fluid model versus discrete element method, Powder technology 273 (2015) 13–18.

[9] W. W. M. Siu, S.-K. Lee, Transient temperature computation of spheres in three-dimensional random packings, International journal of heat and mass transfer 47 (5) (2004) 887–898.

[10] Y. T. Feng, K. Han, C. F. Li, D. R. J. Owen, Discrete thermal element modelling of heat conduction in particle systems: Basic formulations, Journal of Computational Physics 227 (10) (2008) 5072–5089.

[11] Y. T. Feng, K. Han, D. R. J. Owen, Discrete thermal element modelling of heat conduction in particle systems: pipe-network model and transient analysis, Powder Technology 193 (3) (2009) 248–256.

[12] J. He, Q. Liu, Z. Wu, X. Xu, Modelling transient heat conduction of granular materials by numerical manifold method, Engineering Analysis with Boundary Elements 86 (2018) 45 – 55.

[13] E. Tsotsas, Particle-particle heat transfer in thermal DEM: Three competing models and a new equation, International Journal of Heat and Mass Transfer 132 (2019) 939–943.

[14] Y. Liang, H. Niu, Y. Lou, Expression for ETC of the solid phase of randomly packed granular materials, Applied Thermal Engineering 109 (2016) 44–52.

[15] W. Van Antwerpen, C. G. Du Toit, P. G. Rousseau, A review of correlations to model the packing structure and effective thermal conductivity in packed beds of mono-sized spherical particles, Nuclear Engineering and design 240 (7) (2010) 1803–1818.

[16] C.-W. Nan, R. Birringer, D. R. Clarke, H. Gleiter, Effective thermal conductivity of particulate composites with interfacial thermal resistance, Journal of Applied Physics 81 (10) (1997) 6692–6699.

[17] M. H. Esfe, S. Saedodin, S. Wongwises, D. Toghraie, An experimental study on the effect of diameter on thermal conductivity and dynamic viscosity of Fe/water nanofluids, Journal of Thermal Analysis and Calorimetry 119 (3) (2015) 1817–1824.

[18] C. H. Li, G. P. Peterson, Experimental investigation of temperature and volume fraction variations on the effective thermal conductivity of nanoparticle suspensions (nanofluids), Journal of Applied Physics 99 (8) (2006) 84314.

[19] Y. Liang, Expression for effective thermal conductivity of randomly packed granular material, International Journal of Heat and Mass Transfer 90 (2015) 1105–1108.

[20] O. B. Kovalev, A. V. Gusarov, Modeling of granular packed beds, their statistical analyses and evaluation of effective thermal conductivity, International Journal of Thermal Sciences 114 (2017) 327–341.

[21] A. Arzhang, A survey on christoffel–darboux type identities of legendre, laguerre and hermite polynomials, Mathematical Sciences 9 (4) (2015) 193–197.

[22] Y. Tsuji, T. Tanaka, T. Ishida, Lagrangian numerical simulation of plug flow of cohesionless particles in a horizontal pipe, Powder technology 71 (3) (1992) 239–250.

[23] P. Jalali, M. Nikku, T. Hyppanen, Particle-cloud drag force in dilute particle systems: discrete element method versus Eulerian simulations, Industrial & Engineering Chemistry Research 52 (11) (2013) 4342–4350.

[24] G. K. Batchelor, R. W. O'brien, Thermal or electrical conduction through a granular material, Proceedings of the Royal Society of London. A. Mathematical and Physical Sciences 355 (1682) (1977) 313–333.

[25] H. S. Carslaw, J. C. Jaeger, Conduction of heat in solids, Oxford: Clarendon Press, 1959, 2nd ed.

[26] M. M. Yovanovich, Thermal contact resistance across elastically deformed spheres., Journal of Spacecraft and Rockets 4 (1) (1967) 119–122.

[27] C. Argento, D. Bouvard, Modeling the effective thermal conductivity of random packing of spheres through densification, International Journal of Heat and Mass Transfer 39 (7) (1996) 1343 – 1350.

[28] J. K. Ott, Modeling the microstructural and micromechanical influence on effective properties of granular electrode structures: with regard to solid oxide fuel cells and lithium ion batteries (2015).

[29] O. Birkholz, Y. Gan, M. Kamlah, Modeling the effective conductivity of the solid and the pore phase in granular materials using resistor networks, Powder Technology 351 (2019) 54 – 65.

[30] W. Dai, D. Hanaor, Y. Gan, The effects of packing structure on the effective thermal conductivity of granular media: A grain scale investigation, International Journal of Thermal Sciences 142 (2019) 266–279.

[31] M. Moscardini, Y. Gan, S. Pupeschi, M. Kamlah, Discrete element method for effective thermal conductivity of packed pebbles accounting for the Smoluchowski effect, Fusion Engineering and Design 127 (2018) 192–201.

[32] A. R. Peeketi, M. Moscardini, A. Vijayan, Y. Gan, M. Kamlah, R. K. Annabattula, Effective thermal conductivity of a compacted pebble bed in a stagnant gaseous environment: An analytical approach together with dem, Fusion Engineering and Design 130 (2018) 80 – 88.

[33] M. Kwapinska, G. Saage, E. Tsotsas, Continuous versus discrete modelling of heat transfer to agitated beds, Powder technology 181 (3) (2008) 331–342.

[34] I. Terreros, I. Iordanoff, J.-L. Charles, Simulation of continuum heat conduction using DEM domains, Computational Materials Science 69 (2013) 46–52.

[35] H. Zhong, J. R. Lukes, Interfacial thermal resistance between carbon nanotubes: molecular dynamics simulations and analytical thermal modeling, Physical Review B 74 (12) (2006) 125403.